RSC Advances

PAPER

View Article Online
View Journal | View Issue

Cite this: *RSC Adv.*, 2021, **11**, 6943

TiO_2-Based photocatalyst modified with a covalent triazine-based framework organocatalyst for carbamazepine photodegradation

Xiaofang Chao, Yaqian Xu, Hui Chen, Diejing Feng, Jinxing Hu and Yan Yu *

Received 12th November 2020
Accepted 29th December 2020

DOI: 10.1039/d0ra09619a

rsc.li/rsc-advances

A novel fluorine-doped TiO_2 ($TiO_{2-X}F_X$) heterojunction semiconductor photocatalyst was synthesised using covalent triazine-based frameworks (CTFs) at different weight ratios. X-ray photoelectron spectroscopy revealed that doping with CTFs shifts the value of the $TiO_{2-X}F_X$ catalyst to a lower binding energy, which led to the bandgap narrowing. From the results of the photocatalytic activity and Fourier-transform infrared spectroscopy, a rise in carbamazepine (CBZ) adsorption under dark conditions and an increased intensity of characteristic triazine units after exfoliation were observed, which indicated that the addition of nanosheet CTFs would increase the number of active sites. Furthermore, the results showed that the $TiO_{2-X}F_X$/CTFs photocatalyst was almost 5.5 times better than pure $TiO_{2-X}F_X$ in the removal of CBZ under visible light owing to the narrowed bandgap, the increased active sites, the quick separation of photo-generated carriers, and improved light absorption. A mechanism for photodegradation of CBZ with the $TiO_{2-X}F_X$/CTFs photocatalyst was proposed.

Introduction

TiO_2-Based semiconductor photocatalysts have been widely studied owing to their low toxicity, low-cost, and high physicochemical stability.[1–8] However, the main disadvantages of TiO_2-based photocatalysts are their wide bandgaps (3.0 eV for rutile and 3.2 eV for anatase),[1] and high electron–hole pair recombination rates.[9,10] Therefore, doping with metal or nonmetal elements, such as transition metals and nonmetal anions, has been introduced to avoid these disadvantages.[11–14] However, anionic dopants such as N-doped TiO_2 reduce the photocatalytic activity if the nitrogen content exceeds a certain value.[15] It was observed that F-doped TiO_2 only had a slight effect on narrowing the bandgap.[1] Transition-metal cations inefficiently separate electron and hole pairs, as they present recombination centres for photocatalytic carriers.[16,17] Moreover, metal doping can have the drawback of thermal instability.[18] Therefore, the synergistic effect with other organic semiconductor catalysts, such as metal–organic frameworks (MOFs)[19,20] and covalent organic frameworks (COFs), can lower the bandgap and lower contamination.[21–24]

Among multiple attractive organic semiconductors photocatalysts, covalent triazine-based frameworks (CTFs), which possess a wide visible-light adsorption band, a tunable band structure,[25] high chemical and thermal stability, low toxicity, a relatively narrow bandgap (2.4 eV),[27–29] and cheap,[26] have been considered as a suitable co-catalyst for TiO_2-based photocatalysts. However, CTFs have similar problems, such as fast photogenerated carrier recombination, to other photocatalysts.[30–32] The synthesis of heterostructures could enhance the separation of the electron–hole pairs,[33–40] thus improving the photocatalytic performance.

In this work, we have modified $TiO_{2-X}F_X$ with CTFs using different weight ratios. The synergistic effect of $TiO_{2-X}F_X$/CTFs was investigated through photocatalytic degradation of a typical pharmaceutical carbamazepine (CBZ) under simulated sunlight irradiation (λ > 420 nm). Moreover, physicochemical characterisation, such as scanning electron microscopy (SEM), Brunauer–Emmett–Teller (BET) N_2 adsorption–desorption, X-ray diffraction (XRD), Fourier-transform infrared spectroscopy (FTIR), and X-ray photoelectron spectroscopy (XPS) were performed and discussed.

Experimental methods

Materials

Tetrabutyl titanate ($C_{16}H_{36}O_4Ti$), 1,4-dicyanobenzene (DCB), trifluoromethanesulfonic acid (TFMS), *N*,*N*-dimethylformamide (DMF), potassium monopersulfate triple salt (PMS, $KHSO_5 \cdot 0.5KHSO_4 \cdot 0.5K_2SO_4$), CBZ, methanol, and sodium hydroxide (NaOH) were supplied by Shanghai Aladdin Biochemical Technology Co., Ltd. Ethanol (EtOH) was obtained from Shanghai Titan Scientific Co., Ltd. Hydrofluoric Acid (HF) was purchased from Kunshan Jincheng Reagent Co., Ltd.

College of Science & Technology Ningbo University, Ningbo University, Ningbo City, China. E-mail: 2111405018@zjut.edu.cn

Synthesis of $TiO_{2-x}F_X$

The fluorine-doped TiO_2 ($TiO_{2-x}F_X$) nanosheets were fabricated by a simple hydrothermal method. $C_{16}H_{36}O_4Ti$ (50 mL) was dissolved in a HF solution (40 wt%, 10 mL), and the mixture was heated in a Teflon-lined autoclave (100 mL) at 240 °C for 24 h after stirring for 30 min at ambient temperature. The precipitation products were obtained using centrifugation and washed three times with ethanol and ultrapure water. The sky blue photocatalyst was obtained after drying in an oven at 80 °C for 12 h.

Synthesis of CTFs

DCB (98 wt%, 4 mmol) was dissolved in TFMS (2.5 mL) under N_2 at 0 °C. Then silica microspheres (0.5 g) were added to the mixture with continuous stirring for 1.5 h at 0 °C. Thereafter, the synthesised products (SiO_2@CTFs), were heated to 100 °C for 20 min, obtained by centrifugation, and washed several times with ultrapure water and ethanol. Subsequently, the composite was dried in a vacuum overnight at 60 °C. H-CTF-Na photocatalysts were synthesised with NaOH (0.5 M) under hydrothermal conditions for 5 h at 60 °C. The products were obtained following centrifugation, washing with ultrapure water and ethanol until neutral, and then dried in a vacuum for 12 h at 60 °C.

Synthesis of $TiO_{2-x}F_X$/CTFs heterojunction photocatalyst

Two types of semiconductor photocatalysts were synthesised through different synthesis methods. In brief, a $TiO_{2-x}F_X$/CTFs van der Waals heterojunction was produced using an ultrasonic and mechanical method. The $TiO_{2-x}F_X$/CTFs mixture was added into a DMF aqueous dispersion (50 mL) and stirred for 2 h. Thereafter, the sample was sonicated for 1 h, washed with ethanol three times, and finally dried in a vacuum overnight at 50 °C. To optimise the photocatalytic characteristic, $TiO_{2-x}F_X$/CTFs was synthesised with three different weight ratios between $TiO_{2-x}F_X$ and CTFs (1 : 0.2, 1 : 0.5, and 1 : 1).

Characterisation

The crystal structures of the synthesised composites were examined using XRD (X'Pert Pro MPD, Panalytical, Netherlands) with a Cu Kα X-ray radiation source (60 kV and 55 mA). The morphology and textural properties of different samples were determined using SEM (SU8010, Hitachi, Japan). The Brunauer–Emmett–Teller (BET) was used to record the surface area with N_2 adsorption–desorption isotherms on an ASAP 2020 system (Micromeritics, USA). FTIR spectra (Thermo Scientific, USA) was measured on a Nicolet iS 10 spectrometer. XPS (Thermo Scientific K-Alpha, USA) was recorded to analyse the surface chemical environments. The excitation source was Al Kα ($h\nu$ = 1486.6 eV) and the X-ray gun was operated at 72 W (12 kV, 6 mA).

Photocatalytic reaction

The photocatalytic activity of three prepared $TiO_{2-x}F_X$/CTFs catalysts and pure $TiO_{2-x}F_X$ were examined through the photodegradation of carbamazepine (CBZ) in aqueous solutions with simulated sunlight irradiation. The solution of CBZ (5 mg L^{-1}) was prepared and diluted with deionised water to desirable experimental concentrations. The experiments were performed using a CEL-S500/350 Xe lamp (Beijing CeauLight Co., Ltd, China) with an optical cut-off filter (λ > 420 nm). A thermostat (DFY-5L/40, Gongyi City Yuhua Instrument Co., Ltd, China) was applied to preserve the invariable temperature at 25 °C.

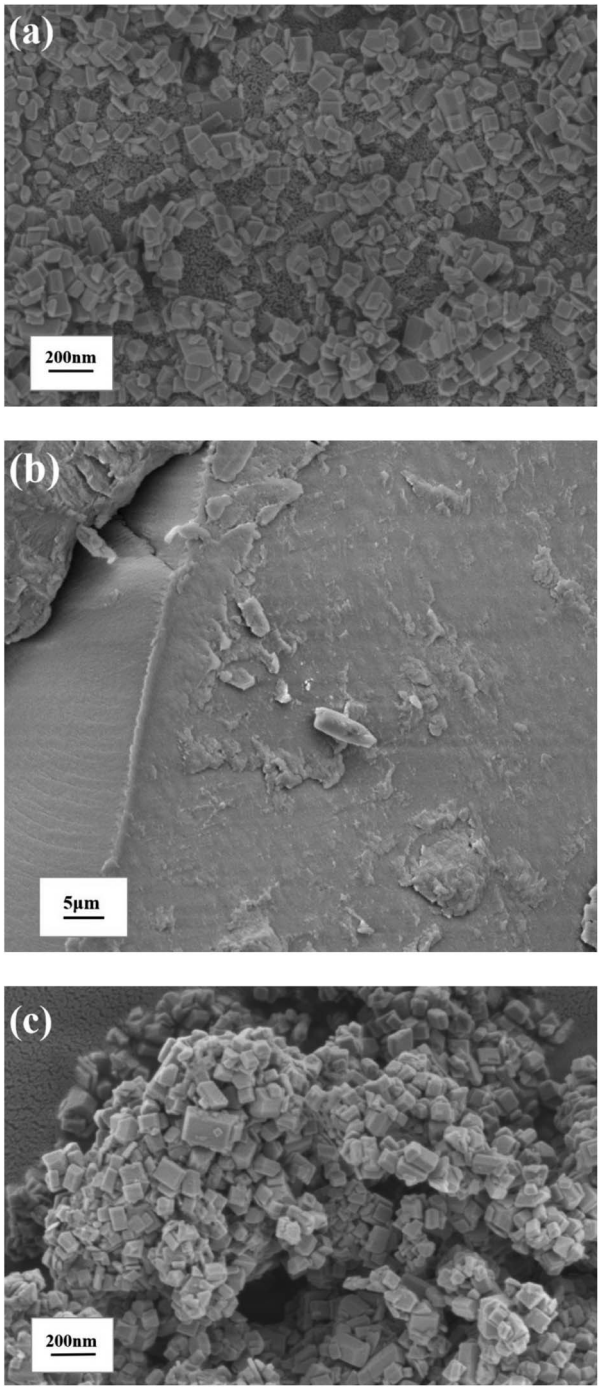

Fig. 1 Scanning electron microscopy images of (a) $TiO_{2-x}F_X$, (b) CTFs and (c) $TiO_{2-x}F_X$/CTFs.

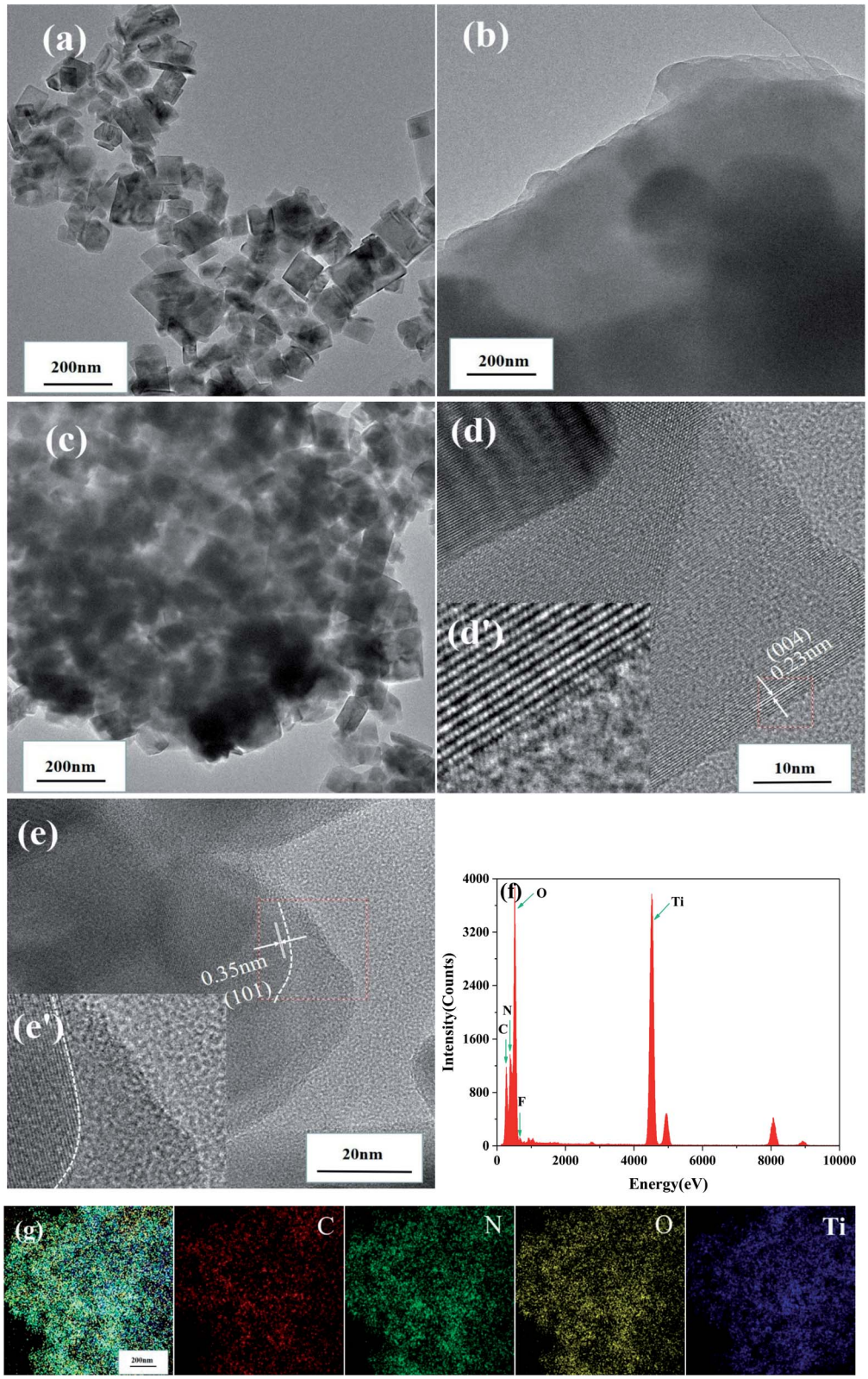

Fig. 2 Transmission electron spectroscopy images of (a) $TiO_{2-X}F_X$, (b) CTFs and (c) $TiO_{2-X}F_X$/CTFs (1 : 1), (d and e) inverse fast Fourier transform images (the insets) (f) energy-dispersive X-ray spectroscopy and (g) element mapping images of $TiO_{2-X}F_X$/CTFs (1 : 1).

Before mixing with the four different photocatalysts, PMS (40 mg) was added to a CBZ aqueous solution (100 mL, 5 mg L^{-1}) in a photo-reactor. The suspension was continuously stirred under dark conditions for 30 min at 25 °C to establish an adsorption–desorption equilibrium. Thereafter, the Xe lamp was turned on to start the photocatalytic reaction, and then during the

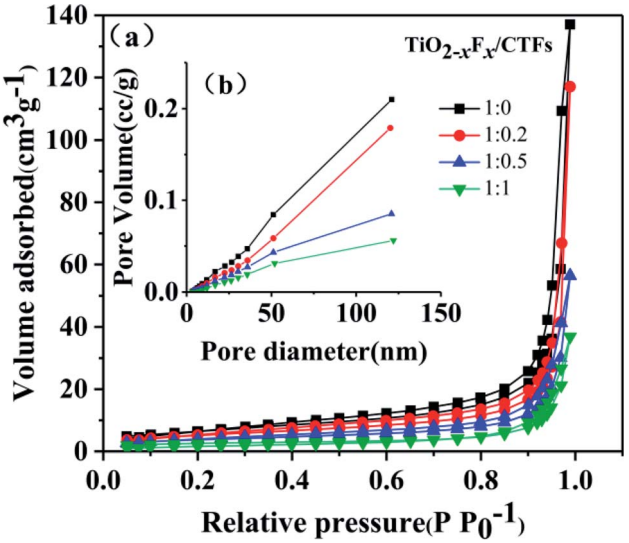

Fig. 3 (a) N_2 adsorption–desorption isotherms and (b) pore-size distribution of the $TiO_{2-x}F_X$/CTFs photocatalysts.

Table 1 Textural parameters of pure $TiO_{2-x}F_X$ and $TiO_{2-x}F_X$/CTFs

$TiO_{2-x}F_X$/CTFs	BET surface areas ($m^2\ g^{-1}$)	Total pore volume (cc g^{-1})	Average pore diameter (nm)
1 : 0	23.283	0.212	36.42
1 : 0.2	18.785	0.1811	38.56
1 : 0.5	13.523	0.08727	25.81
1 : 1	9.357	0.057	24.37

photocatalytic reaction, aliquots (1.0 mL) were taken and filtrated at certain intervals using a syringe filter (0.22 μm). The concentration of the filtered solution was detected using mass spectrometry (Agilent HPLC-1260 with a C_{18} column (4.6 mm × 150 mm, 4 μm) and a UV detector). The mobile phase was methanol (80%) in ultrapure water (flow rate of 1.0 mL min^{-1}), the column temperature was 40 °C, and the detection wavelength was 285 nm.

Result and discussion

Fig. 1 showed SEM images of pure $TiO_{2-x}F_X$, pure CTFs and the combination of two catalysts. In Fig. 1a, $TiO_{2-x}F_X$ demonstrated a uniform octahedral sheet structure[1] and CTFs displayed a structure with a rough surface (Fig. 1b). SEM images of $TiO_{2-x}F_X$/CTFs heterojunctions were shown in Fig. 1c, in which the agglomerate structure of $TiO_{2-x}F_X$ was exhibited.

TEM

Transmission electron microscopy (TEM) was performed to reveal the crystallographic properties of pristine $TiO_{2-x}F_X$, pristine CTFs, and the synthesised $TiO_{2-x}F_X$/CTFs with a weight ratio 1 : 1 at an atomic scale (Fig. 2a–c). TEM images indicated that $TiO_{2-x}F_X$ possesses the regular octahedral shape (Fig. 2a), the CTFs edge showed a layered structure (Fig. 2b), and the $TiO_{2-x}F_X$/CTFs (1 : 1) catalyst demonstrated a combination of the two substances (Fig. 2c). As shown in Fig. 2d and e, to further investigate the structure of $TiO_{2-x}F_X$/CTFs (1 : 1), we enlarged the selected regions (red box) with the inverse fast Fourier transform (IFFT) images (Fig. 2d and e). The IFFT image revealed regular lattice fringes with a *d*-spacing of 0.23 and 0.35 nm, corresponding to the (004) plane and (101) plane of anatase.[41] The IFFT image also displayed the CTFs layer extending to the border in Fig. 2e.

Furthermore, energy-dispersive X-ray spectroscopy (EDS) (Fig. 2f) revealed that $TiO_{2-x}F_X$/CTFs mainly consists of C, N, O, Ti, and F. The element mapping images of $TiO_{2-x}F_X$/CTFs (1 : 1) (Fig. 2g) showed that C (deep red), N (green), O (yellow), and Ti (deep blue) were evenly dispersed, which confirmed that $TiO_{2-x}F_X$ and CTFs were well combined. These results were further demonstrated by XRD and XPS analyses.

BET

N_2 adsorption–desorption measurements shown in Fig. 3 indicated the porosity of the four photocatalysts. The samples exhibited a type IV isotherm and H3 hysteresis loop.[1] The plunge in the desorption curve and the hysteresis loop at high relative pressure indicated the mesoporosity of the samples (Fig. 3a). The pore size distributions (Fig. 3b), which were acquired using the BJH (Barret–Joyner–Halenda) method, indicated that the samples have a wide pore distribution range (10–130 nm).

The BET specific surface area, total pore volume, and average pore diameter of the four catalysts were shown in Table 1. With an increase in CTF concentration, a slight decrease in BET surface area and pore volume was seen. This indicated that the addition of CTFs might result in a relatively dense organic framework through agglomeration, which was indicated by SEM images, and led to smaller mesopore size and lower surface area.

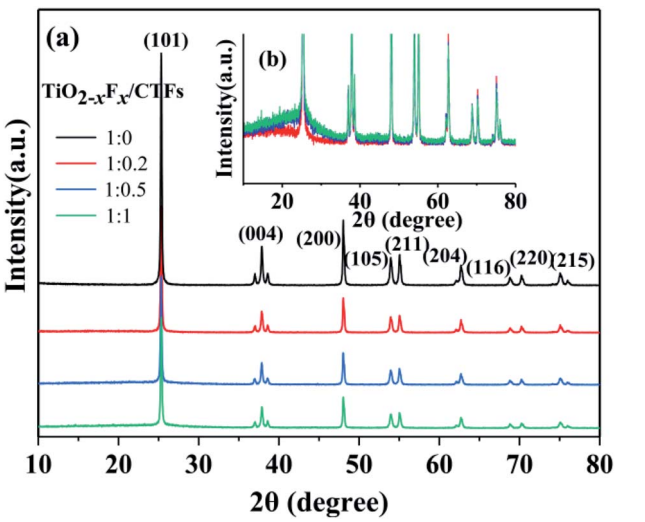

Fig. 4 (a) X-ray diffraction patterns of different photocatalysts and (b) enlarged XRD patterns of the $TiO_{2-x}F_X$/CTFs photocatalysts with different weight ratios.

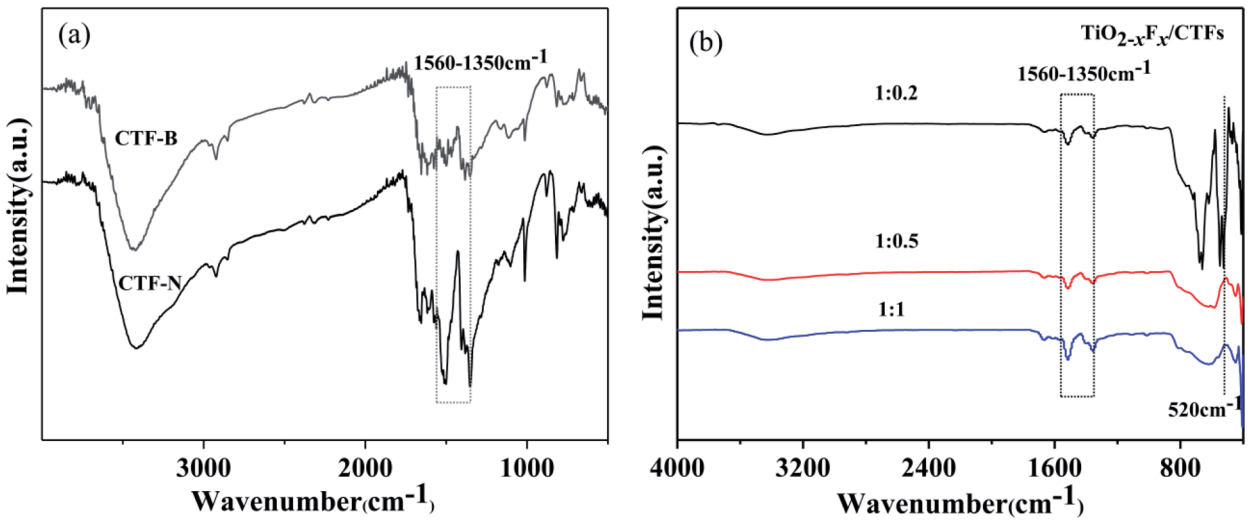

Fig. 5 (a) Fourier-transform infrared (FTIR) spectra of bulk CTFs (CTF-B) and nanosheet CTFs (CTF-N) and (b) FTIR spectra of the $TiO_{2-X}F_X$/CTFs photocatalysts with weight ratios 1 : 0.2 (black), 1 : 0.5 (red), and 1 : 1 (blue).

XRD

Three $TiO_{2-X}F_X$/CTFs photocatalysts with different weight ratios and a pure $TiO_{2-X}F_X$ catalyst were analysed using XRD. Fig. 4a showed the diffraction peaks which corresponded to the TiO_2 crystalline phase of anatase. The diffraction peaks at approximately 25.3°, 37.8°, 48.1°, 53.9°, 55.1°, 62.7°, 68.7°, 70.3°, and 75.1° correspond to the crystal planes of (101), (004), (200), (105), (211), (204), (116), (220), and (215), respectively.[42] An increase in the characteristic peak for CTFs was observed in the XRD patterns (Fig. 4b). The main increased intensity was observed at around 27.0°, which indicated the crystal plane of the π-conjugated bond rings.[43] These results indicated the presence of both photocatalysts. With decreasing weight ratio of $TiO_{2-X}F_X$/CTFs from 1 : 0.2 to 1 : 1, the intensity of anatase decreased. Meanwhile, the intensity of CTFs was improved.

FTIR

To investigate the impact of exfoliation on bulk CTFs through sonication, FTIR was measured. As shown in Fig. 5a, the characteristic bands for triazine (1560–1350 cm^{-1}) were seen for bulk CTFs and nanosheet CTFs.[26,44–47] Compared with bulk CTFs, an increased intensity for the adsorption peak corresponding to triazine in the nanosheet CTFs was observed, which indicated that by exfoliating bulk CTFs to form nanosheet CTFs, triazine was exposed on the surface of CTFs. FTIR analysis of the photocatalysts indicated the successful formation of triazine (Fig. 5b). All samples showed a strong adsorption band at approximately 1560–1350 cm^{-1}, which corresponded to the triazine unit.[26,44–47] A strong adsorption band at approximately 520 cm^{-1}, which corresponded to the Ti–O stretching band, was demonstrated when the $TiO_{2-X}F_X$/CTFs weight ratio is at 1 : 0.2.[48] However, for the weight ratios 1 : 0.5 and 1 : 1, the Ti–O stretching band was hardly visible.

XPS

The XPS survey spectra of the photocatalysts indicated that they contained C, N, Ti, O, and F (Fig. 6a). As shown in Fig. 6b, the XPS spectra of the C 1s region of the photocatalysts revealed three peaks. The strongest signal at 284.8 eV was assigned to the carbon atoms in aromatic rings and used as the reference carbon for calibrating the XPS instrument.[44] The second peak was at approximately 287.0 eV and was assigned to the N–C=N bond in triazine.[49] The third peak centred at approximately 288.4 eV corresponds to the carbon in C–N groups.[49] The N 1s spectra were resolved into two individual peaks located at around 398.9 eV and 400.0 eV (Fig. 6c), which were assigned to the N atoms in C–N=C of triazine,[26,44] and the pyrrolic-like nitrogen (C–N–C) deriving from the decomposition of triazine, respectively.[50] For the $TiO_{2-X}F_X$/CTFs photocatalyst, the peak at approximately 399.0 eV was shifted to a higher binding energy compared to pristine CTFs.

The O 1s spectra were deconvoluted into two peaks at the binding energies of 529.7 eV and 531.2 eV (Fig. 6d), which were assigned to Ti–O in $TiO_{2-X}F_X$[1] and to surface hydroxyl in adsorbed H_2O molecules, respectively.[41,51] The oxygen peak located at 529.7 eV was shifted slightly to lower binding presence of oxygen vacancies.[41] The Ti 2p XPS spectra were shown in Fig. 6e and could be fitted by four peaks at approximately 458.4 eV, 458.9 eV, 463.3 eV, and 464.5 eV. The peaks at binding energies of 458.9 and 464.5 eV corresponded to the signals of Ti $2p_{1/2}$ and Ti $2p_{3/2}$ of Ti^{4+}, respectively, whereas the two peaks at 458.4 eV and 463.3 eV corresponded to the signals of Ti $2p_{1/2}$ and Ti $2p_{3/2}$ of Ti^{3+}, respectively.[52] The Ti 2p region was shifted slightly to lower binding energy compared with pristine $TiO_{2-X}F_X$.

Therefore, by comparing the $TiO_{2-X}F_X$/CTFs photocatalyst with pristine $TiO_{2-X}F_X$ and CTFs, the N 1s binding energy increased, whereas the Ti 2p binding energy decreased. These shifted peaks indicated a strong synergetic effect between $TiO_{2-X}F_X$ and CTFs and the transference of electrons from CTFs to $TiO_{2-X}F_X$, which indicated the successful combination of the two photocatalysts.

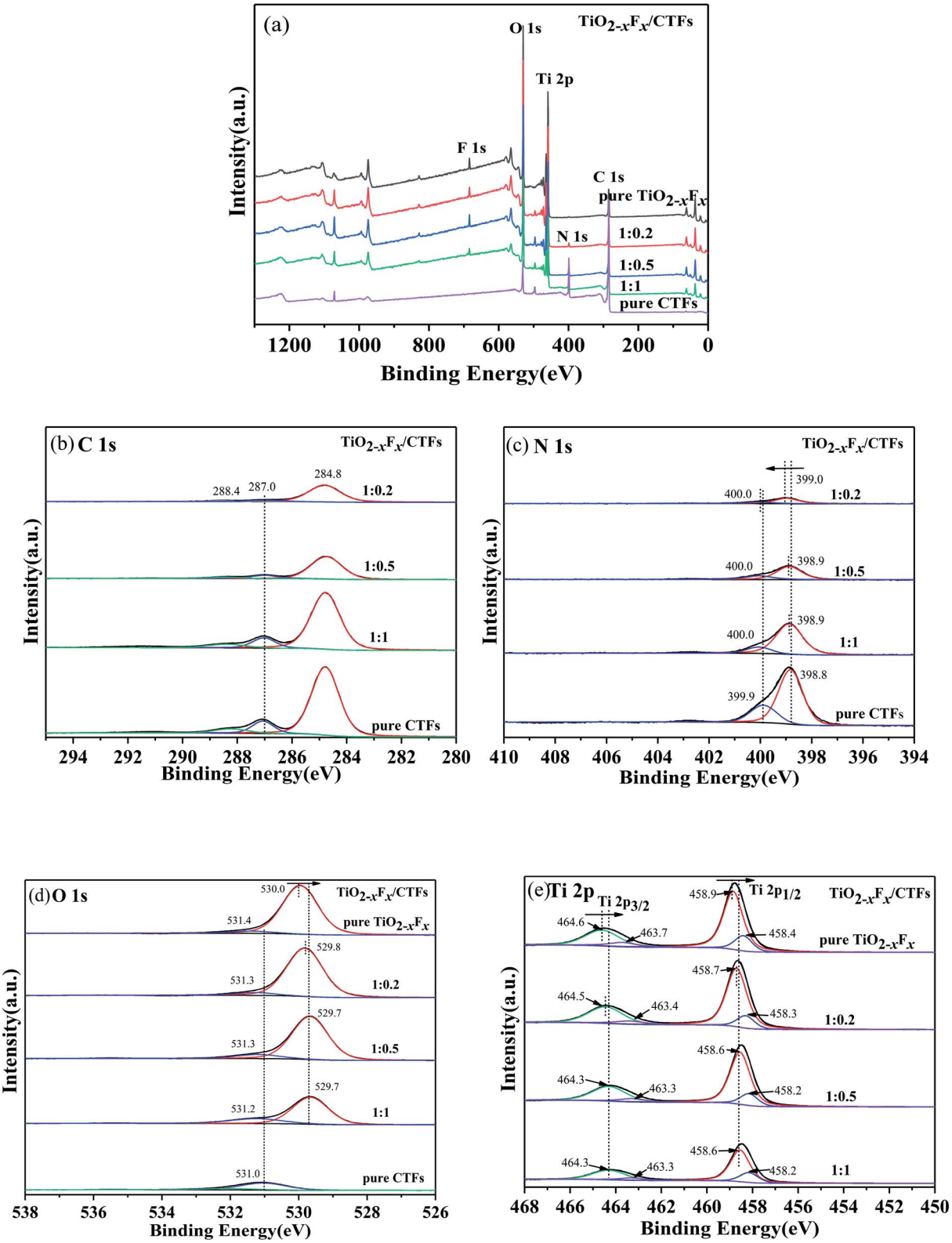

Fig. 6 (a) X-ray survey and high-resolution spectrum for (b) C 1s, (c) N 1s, (d) O 1s, and (e) Ti 2p.

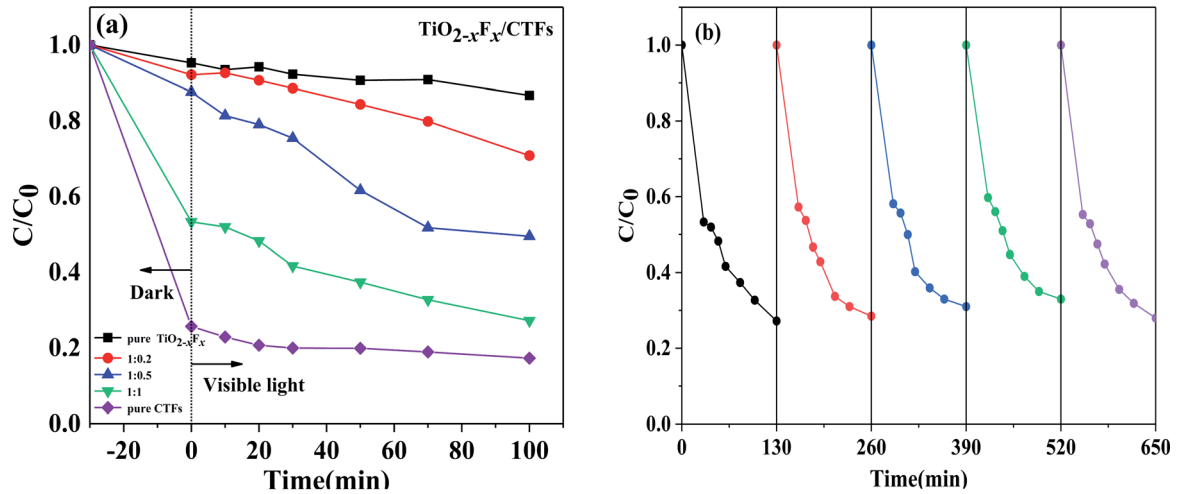

Fig. 7 (a) Photocatalytic degradation of carbamazepine over the five catalysts under visible-light irradiation (λ > 420 nm) (b) stability test of $TiO_{2-X}F_X$/CTFs catalyst (1 : 1) for carbamazepine photodegradation under visible-light irradiation (λ > 420 nm).

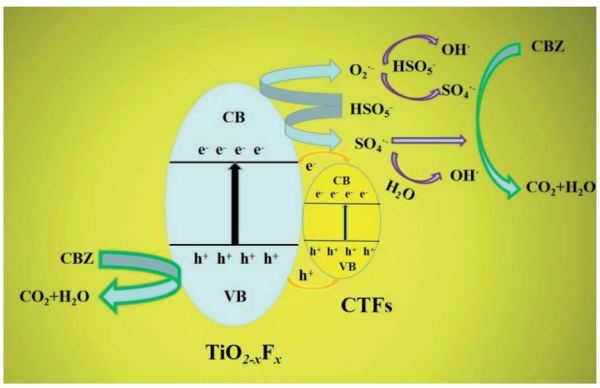

Fig. 8 Schematic showing the mechanism for carbamazepine (CBZ) photocatalytic degradation on a $TiO_{2-X}F_X$/CTFs heterojunction. CB and VB are the conduction band and valence band, respectively.

The effect of $TiO_{2-X}F_X$/CTFs on CBZ photocatalytic degradation

To investigate the photocatalytic activity of the catalysts, the degradation of CBZ in the presence of PMS irradiated under visible light was performed. It is well-known that PMS cannot degrade CBZ effectively without a catalyst. The results of these measurements were shown in Fig. 7a.

After treatment under dark conditions for 30 min, the $TiO_{2-X}F_X$/CTFs catalysts had a higher CBZ adsorption than pure $TiO_{2-X}F_X$ catalyst (approximately 4.7%). Notably, for the catalyst with 50% CTF, the degradation efficiency was 46.7%, which is almost 10 times higher than pure $TiO_{2-X}F_X$. In this study, the degradation efficiency of the $TiO_{2-X}F_X$/CTFs catalyst was enhanced owing to the presence of Ti^{3+} and triazine units, which provide a large number of active sites,[51–53] thus improving CBZ absorption.

Under visible light, the degradation efficiency of the $TiO_{2-X}F_X$ and CTFs catalysts with weight ratios 1 : 0, 1 : 0.2, 1 : 0.5, 1 : 1, and 0 : 1 was 13.3%, 29.2%, 50.5%, 72.8%, and 82.7%, respectively, within 100 min of irradiation. These results showed that there was an increase in CBZ degradation with an increase in the weight ratio of CTFs. In addition, the trend of CBZ degradation efficiency of the pure CTFs was similar to that of the pure $TiO_{2-X}F_X$, there was no significant degradation trend when compared to the $TiO_{2-X}F_X$/CTFs heterojunction catalyst in the visible light region, which indicated that the synthesis of heterostructures could decrease the recombination of the electron–hole pairs, thus improving photocatalytic performance.

The bandgaps of $TiO_{2-X}F_X$ and CTFs are 3.13 eV[1] and 1.85–1.50 eV,[54] respectively. The shift of the O 1s and Ti 2p XPS peaks to lower binding energy demonstrated that the presence of CTFs could decrease the bandgap. As mentioned above, the cooperative effect of CTFs not only exposes a large number of active sites, but also significantly narrows the bandgap, thus decreasing the photo-generated charge transfer distance, and increasing visible light adsorption, so that the recombination of the electrons and holes is impeded, which improves the photocatalytic activity.

To further evaluate the stability of the $TiO_{2-X}F_X$/CTFs heterojunction photocatalyst, recyclability tests for CBZ photodegradation were performed on a representative $TiO_{2-X}F_X$/CTFs catalyst (1 : 1). As shown in Fig. 7b, no obvious decrease in the removal efficiency of CBZ could be observed for 650 min under visible-light irradiation over five continuous runs. The results exhibited the recyclability and stability of the $TiO_{2-X}F_X$/CTFs photocatalyst.

Mechanism for CBZ photocatalytic degradation on $TiO_{2-X}F_X$/CTFs

A possible mechanism for CBZ photocatalytic degradation on $TiO_{2-X}F_X$/CTFs is presented in Fig. 8. After exposure to the Xe lamp, photogenerated carriers are excited from the valence band into the conduction band of catalysts. PMS quickly captures the photo-generated electrons on the surface of the

catalysts, and transfers into $O_2^{\bullet-}$ and $SO_4^{\bullet-}$ radicals form. Intermediate $O_2^{\bullet-}$ could further react with PMS to produce $^{\bullet}OH$ and $SO_4^{\bullet-}$ radicals. As for $SO_4^{\bullet-}$, it may oxidise H_2O to form a $^{\bullet}OH$ radical. After a series of reactions, PMS is oxidised to generate chiefly $^{\bullet}OH$ and $SO_4^{\bullet-}$ radicals.[54] In addition, CBZ may be oxidised by photogenerated h^+ directly. So CBZ could be degraded in the presence of $^{\bullet}OH$, $SO_4^{\bullet-}$ and h^+ oxidative species to finally transform into CO_2 and H_2O *via* a chain of reactions.

As is shown in Fig. 8, the conduction band of CTFs (0.2 eV)[54] is more positive than $TiO_{2-X}F_X$ (−0.5 eV),[1] whereas the valence band of CTFs (1.48–1.83 eV) is more negative than $TiO_{2-X}F_X$ (2.63 eV). Therefore, the photogenerated electrons and holes could transfer easily from the surface of $TiO_{2-X}F_X$ to the surface of CTFs. In this case, the migration of e^- and h^+ between the two photocatalysts could effectively separate photo-charged carriers and further favour visible light absorption.

Conclusions

In summary, $TiO_{2-X}F_X$/CTFs van der Waals heterojunction photocatalysts were successfully synthesised using a stirring and sonication method. A synergetic effect of heterostructure catalysts was observed through the photocatalytic degradation of CBZ. The removal efficiency of CBZ was influenced by the $TiO_{2-X}F_X$/CTFs weight ratio and reaction time. The XPS results suggested a strong interaction between $TiO_{2-X}F_X$ and CTFs and electron transfer between the two photocatalysts. The synergistic effect results in a smaller bandgap, improved light adsorption, and the separation of electrons and holes. In addition, CBZ adsorption under dark conditions was enhanced compared to $TiO_{2-X}F_X$ owing to the increased number of active sites, which could be observed using FTIR and XPS. Furthermore, this highly efficient, low toxic, cheap, and high performing photocatalyst provides a novel, green, and facile method for organic pollutant treatment.

Conflicts of interest

There are no conflicts to declare.

Acknowledgements

This study was sponsored by the 68th Financial Grant from China Postdoctoral Science Foundation (no. 2020M681809), Preferential Funding Projects for Postdoctoral Scientific Research in Zhejiang Province (no. ZJ2020083) and K. C. Wong Magna Fund in Ningbo University.

References

1 Z. Q. He, J. T. Tang, J. Shen, J. M. Chen and S. Song, *Appl. Surf. Sci.*, 2016, **364**, 416–427.
2 M. Pelaez, N. T. Nolan, S. C. Pillai, M. K. Seery, P. Falaras, A. G. Kontos, P. S. M. Dunlop, J. W. J. Hamilton, J. A. Byrne and K. O'Shea, *Appl. Catal., B*, 2012, **125**, 331–349.
3 C. H. Ao, S. C. Lee, Y. Z. Yu and J. H. Xu, *Appl. Catal., B*, 2004, **54**, 41–50.
4 A. Fujishima, T. N. Rao and D. A. Tryk, *J. Photochem. Photobiol., C*, 2000, **1**, 1–21.
5 I. J. Ochuma, R. P. Fishwick, J. Wood and J. M. Winterbottom, *J. Hazard. Mater.*, 2007, **144**, 627–633.
6 A. C. Rodrigues, M. Boroski, N. S. Shimada, J. C. Garcia, J. Nozaki and N. Hioka, *J. Photochem. Photobiol., A*, 2008, **194**, 1–10.
7 A. Strini, S. Cassese and L. Schiavi, *Appl. Catal., B*, 2005, **61**, 90–97.
8 T. L. Thompson and J. T. Yates, *Chem. Rev.*, 2006, **106**, 4428–4453.
9 B. Tahir, M. Tahir and N. S. Amin, *Appl. Surf. Sci.*, 2015, **338**, 1–14.
10 W. Choi, A. Termin and M. R. Hoffmann, *J. Phys. Chem.*, 1994, **98**, 13669–13679.
11 J. Choi, H. Park and M. R. Hoffmann, *J. Phys. Chem. C*, 2009, **114**, 78–792.
12 X. Chen and C. Burda, *J. Am. Chem. Soc.*, 2008, **130**, 5018–5019.
13 C. Wang, Q. Q. Hu, J. Q. Huang, C. Zhu, Z. H. Deng, H. L. Shi, L. Wu, Z. G. Liu and Y. G. Cao, *Appl. Surf. Sci.*, 2014, **292**, 161–164.
14 M. M. Gui, S. P. Chai and A. R. Mohamed, *Appl. Surf. Sci.*, 2014, **319**, 37–43.
15 K. Wojtaszek, A. Wach, J. Czapla-Masztafiak, K. Tyrala, J. Sa, L. Yıldız Ozer, C. Garlisi, G. Palmisanod and J. Szlachetko, *Synchrotron Radiat.*, 2019, **26**, 145–151.
16 W. Choi, A. Termin and M. R. Hoffmann, *J. Phys. Chem.*, 1994, **98**, 13669.
17 A. L. Linsebigler, G. Q. Lu and J. T. Yates, *Chem. Rev.*, 1995, **95**, 735.
18 W. Choi, A. Termin and M. R. Hoffman, *J. Phys. Chem.*, 1994, **98**, 13669.
19 Q. Zuo, T. Liu, C. Chen, Y. Ji, X. Gong, Y. Mai and Y. Zhou, *Angew. Chem., Int. Ed.*, 2019, **58**, 10198–10203.
20 G. Lan, Y. Quan, M. Wang, G. T. Nash, E. You, Y. Song, S. S. Veroneau, X. Jiang and W. Lin, *J. Am. Chem. Soc.*, 2019, **141**, 15767–15772.
21 I. Gadwal, G. Sheng, R. L. Thankamony, Y. Liu, H. Li and Z. Lai, *ACS Appl. Mater. Interfaces*, 2018, **10**, 12295–12299.
22 Y. Peng, Y. Huang, Y. Zhu, B. Chen, L. Wang, Z. Lai, Z. Zhang, M. Zhao, C. Tan, N. Yang, F. Shao, Y. Han and H. Zhang, *J. Am. Chem. Soc.*, 2017, **139**, 8698–8704.
23 Y. Ying, D. Liu, J. Ma, M. Tong, W. Zhang, H. Huang, Q. Yang and C. Zhong, *J. Mater. Chem. A*, 2016, **4**, 13444–13449.
24 K. Wang, Y. Tang, Q. Jiang, Y. Lan, H. Huang, D. Liu and C. Zhong, *J. Energy Chem.*, 2017, **26**, 902–908.
25 X. Jiang, P. Wang and J. J. Zhao, *J. Mater. Chem. A*, 2015, **15**, 7750–7758.
26 K. K. Wang, H. L. Huang, D. H. Liu, C. Wang, J. P. Li and C. L. Zhong, *Environ. Sci. Technol.*, 2016, **50**, 4869–4876.
27 K. Wang, L. M. Yang, X. Wang, L. Guo, G. Cheng, C. Zhang, S. Jin, B. Tan and A. Cooper, *Angew. Chem., Int. Ed.*, 2017, **56**, 14149–14153.
28 M. Liu, Q. Huang, S. Wang, Z. Li, B. Li, S. Jin and B. Tan, *Angew. Chem., Int. Ed.*, 2018, **57**, 11968–11972.

29 M. Liu, K. Jiang, X. Ding, S. Wang, C. Zhang, J. Liu, Z. Zhan, G. Cheng, B. Li, H. Chen, S. Jin and B. Tan, *Adv. Mater.*, 2019, **31**, 1807865–1807872.
30 P. Pachfule, A. Acharjya, J. Roeser, T. Langenhahn, M. Schwarze, R. Schomacker, A. Thomas and J. Schmidt, *J. Am. Chem. Soc.*, 2018, **140**, 1423–1427.
31 Z. A. Lan, Y. X. Fang, Y. F. Zhang and X. C. Wang, *Angew. Chem., Int. Ed.*, 2018, **57**, 470–474.
32 W. Huang, Z. J. Wang, B. C. Ma, S. Ghasimi, D. Gehrig, F. Laquai, K. Landfester and K. A. I. Zhang, *J. Mater. Chem. A*, 2016, **4**, 7555–7559.
33 J. H. Yang, D. G. Wang, H. X. Han and C. Li, *Acc. Chem. Res.*, 2013, **46**, 1900–1909.
34 F. Y. Wen and C. Li, *Acc. Chem. Res.*, 2013, **46**, 2355–2364.
35 K. Wenderich and G. Mul, *Chem. Rev.*, 2016, **116**, 14587–14619.
36 T. D. Nguyen, Q. T. P. Bui, T. B. Le, T. M. Altahtamouni, K. B. Vu, D. V. N. Vo, N. T. H. Le, T. D. Luu, S. S. Hong and K. T. Lim, *RSC Adv.*, 2019, **9**, 23526–23534.
37 D. Gao, W. Liu, Y. Xu, P. Wang, J. Fan and H. Yu, *Appl. Catal., B*, 2020, **260**, 118190.
38 S. C. Sun, Y. C. Zhang, G. Q. Shen, Y. T. Wang, X. L. Liu, Z. W. Duan, L. Pan, X. W. Zhang and J. J. Zou, *Appl. Catal., B*, 2019, **243**, 253–261.
39 H. G. Yu, R. R. Yuan, D. D. Gao, Y. Xu and J. G. Yu, *Chem. Eng. J.*, 2019, **375**, 121934.
40 M. H. Ai, J. W. Zhang, R. J. Gao, L. Pan, X. W. Zhang and J. J. Zou, *Appl. Catal., B*, 2019, **256**, 117805.
41 X. Xu, L. Lai, T. Zeng, Y. Yu, Z. Q. He, J. M. Chen and S. Song, *J. Phys. Chem. C*, 2018, **122**, 18870–18879.
42 B. N. Bao, X. H. Miao, X. D. Hu, Q. Z. Zhang, X. Y. Jie and X. Y. Zheng, *Catalysts*, 2017, **7**, 117.
43 X. C. Wang, K. Maeda, A. Thomas, K. Takanabe, G. Xin, J. M. Carlsson, K. Domen and M. Antonietti, *Nat. Mater.*, 2009, **8**, 76–80.
44 D. Kong, X. Y. Han, J. J. Xie, Q. S. Ruan, C. D. Windle, S. Gadipelli, K. Shen, Z. M. Bai, Z. X. Guo and J. W. Tang, *ACS Catal.*, 2019, **9**, 7697–7707.
45 P. Katekomol, J. Roeser, M. Bojdys, J. Weber and A. Thomas, *Chem. Mater.*, 2013, **25**, 1542–1548.
46 K. Schwinghammer, S. Hug, M. B. Mesch, J. Senker and B. V. Lotsch, *Energy Environ. Sci.*, 2015, **8**, 3345–3353.
47 K. Wang, H. Huang, D. Liu, C. Wang, J. Li and C. Zhong, *Environ. Sci. Technol.*, 2016, **50**, 4869–4876.
48 H. Q. Sun, Y. Bai, Y. P. Cheng, W. Q. Jin and N. P. Xu, *Ind. Eng. Chem. Res.*, 2006, **45**, 4971–4976.
49 J. Li, P. Liu, H. L. Huang, Y. Li, Y. Z. Tang, D. H. Mei and C. L. Zhong, *ACS Sustainable Chem. Eng.*, 2020, **8**, 5175–5183.
50 Y. Zhu, M. Qiao, W. Peng, Y. Li, G. Zhang, F. Zhang, Y. Li and X. Fan, *J. Mater. Chem. A*, 2017, **5**, 9272e8.
51 N. Bao, Y. Li, Z. Wei, G. Yin and J. Niu, *J. Phys. Chem. C*, 2011, **115**, 5708–5719.
52 B. Qiu, Y. Zhou, Y. Ma, X. Yang, W. Sheng, M. Xing and J. Zhang, *Sci. Rep.*, 2015, **5**, 8591.
53 X. Jiang, P. Wang and J. Zhao, *J. Mater. Chem. A*, 2015, **3**, 7750–7758.
54 T. Zeng, S. Q. Li, Y. Shen, H. Y. Zhang, H. R. Feng, X. L. Zhang, L. X. Y. Li, Z. W. Cai and S. Song, *Appl. Catal., B*, 2019, **257**, 117915.